A Hilbert Transform Spectrometer using a High-T_c Josephson Junction for Bunch Length Measurements at the TTF Linac

M. Geitz, K. Hanke*, P. Schmüser
Deutsches Elektronen-Synchrotron DESY, D-22603 Hamburg
and II. Institut für Experimentalphysik der Universität Hamburg

Y. Y. Divin†, U. Poppe
Institut für Festkörperforschung, Forschungszentrum Jülich GmbH, D-52425 Jülich

V. V. Pavlovskii, V. V. Shirotov, O. Y. Volkov
Institute of Radioengineering & Electronics of RAS, Moscow 103907, Russian Federation

M. Tonutti
III. Physikalisches Institut der RWTH Aachen, D-52056 Aachen

April 1998, 14.4.

Abstract

The longitudinal charge distribution of an electron/positron bunch can be determined from the coherent transition radiation emitted as the bunch crosses a thin metal foil. A Josephson junction made from a thin film of $YBa_2Cu_3O_{7-x}$ on a bicrystal substrate is used as a detector for transition radiation in the millimeter and submillimeter range. The radiation-induced modification of the current-voltage characteristic of the Josephson junction is derived from a scan with and without incident radiation. Multiplying this quantity with the dc bias current and the dc voltage across the junction and applying a Hilbert transformation one obtains the spectral intensity of the radiation and the longitudinal form factor of the bunch. The physical principles of a Josephson junction as a detector for submillimeter radiation are outlined and a first bunch length measurement is presented.

1 Introduction

Future electron-positron linear colliders as well as electron drive linacs for Free Electron Lasers (FEL) in the X-ray regime require the production and acceleration of bunches whose length is in the 50-100 μm range. In the TESLA Test Facility (TTF) linac [1] the short length is achieved in a series of bunch compressors which combine off-crest acceleration of the bunches in an rf cavity - thereby establishing a correlation between the position of a particle inside the bunch and its energy - with a magnetic bypass providing a longer path length for the front (lower-energy) particles than for the back (higher-energy) particles. The correct functioning of these bunch compressors must be verified with diagnostic elements providing sufficient longitudinal resolution.

The standard bunch length measurement consists in determining the time duration of the light pulses generated by the electron bunches when they emit either synchrotron, transition or Čerenkov radiation. Streak cameras are well suited for this purpose down to about a picosecond but they are becoming very costly and less efficient in the 100 femtosecond regime. Here frequency-resolved techniques are adequate such as far-infrared grating spectroscopy [2] or Fourier-transform spectroscopy [3, 4, 5]. If the wavelengths exceed the bunch length, all electrons in the bunch radiate coherently and in that case the longitudinal charge distribution in the bunch can be obtained by Fourier transformation of the measured frequency spectrum. The spectrometers used for such measurements are usually equipped with mechanically movable elements like mirrors or gratings, hence the recording of the entire frequency spectrum may last several minutes and an average over many successive bunches has to be taken.

*present adress: CERN, CH-1211 Geneva 23
†home adress: Institute of Radioengineering & Electronics of RAS, Moscow 103907, Russian Federation

The possibility of high-speed spectroscopy in the millimeter- and submillimeter-wavelength range is offered by Hilbert-transform spectroscopy based on the ac Josephson effect [6]. This technique might also permit single-bunch measurements. The principle is to investigate the modification of the current-voltage characteristic of a Josephson junction due to incident radiation. Applying a Hilbert transformation to this modification the frequency spectrum of the radiation can be derived and, after Fourier transformation, the charge distribution in the bunch can be calculated. It is planned to install a Josephson junction spectrometer for sub-picosecond electron bunch length measurements at the TESLA Test Facility (TTF) linac. The device will be able to determine the length of a selected bunch in a macropulse (averaged over several macropulses) or the average length of all bunches within a single macropulse. In the initial stage it is planned to utilize the transition radiation produced in a thin metal foil. In a later stage it is planned to set up a non-destructive bunch length measurement by using the wake field radiation emitted at impedance changes of the vacuum chamber.

In Section 2, the determination of the bunch form factor using transition radiation is described. This is followed by a description of the principle of Hilbert-transform spectroscopy. In Section 4 the results of a first exploratory bunch length measurement are presented. The mathematical derivation of the current-voltage characteristic of a Josephson junction without and with incident microwave radiation is summarized in the Appendix.

2 Principle of the Bunch Length Measurement

2.1 Determination of the Bunch Form Factor using Transition Radiation

Transition radiation is produced when relativistic charged particles pass the interface between two materials of different dielectric properties. The radiation is emitted in both forward and backward direction. By arranging the radiator, here a thin aluminum foil, at an angle of 45° with respect to the electron beam direction, the "backward" radiation is emitted at 90° with respect to the electron beam and can be easily extracted for diagnostics purposes. The spectral intensity emitted by a bunch consisting of N particles can be expressed as

$$I_{tot}(\lambda) = I_1(\lambda)[N + N(N-1)\,|f(\lambda)|^2] \tag{1}$$

where $I_1(\lambda)$ is the intensity radiated by a single electron at the given wavelength λ and $f(\lambda)$ is the bunch form factor [7, 8, 9], defined as the three-dimensional Fourier transform of the normalized charge distribution $\rho(\mathbf{r})$

$$f(\lambda) = \int \rho(\mathbf{r}) \exp\left(\frac{2\pi i(\mathbf{n}\cdot\mathbf{r})}{\lambda}\right) d^3r\,. \tag{2}$$

Here $\mathbf{n} = \mathbf{n}(\mathbf{r})$ is a unit vector pointing from the volume element d^3r at position $\mathbf{r}$ inside the bunch towards the observer. Equation (1) shows that the intensity spectrum emitted by a bunch of N particles contains two parts: the incoherent term $N \cdot I_1(\lambda)$ where all N electrons radiate independently, and the coherent part $N(N-1)|f(\lambda)|^2 \cdot I_1(\lambda)$ where the particles radiate with synchronized phase. Only this latter part contains the information on the spatial distribution of charge inside the bunch.
For simplicity we choose the direction of observation along the z-axis (beam direction) and neglect the transverse charge distribution. Then (2) simplifies to

$$f(\lambda) = \int_{-\infty}^{+\infty} \rho(z) \exp\left(\frac{2\pi i z}{\lambda}\right) dz \tag{3}$$

and the form factor depends only on the longitudinal charge distribution $\rho(z)$. Due to the normalization

$$\int_{-\infty}^{+\infty} \rho(z)\, dz = 1 \tag{4}$$

the absolute magnitude of the form factor can have values between 0 and 1.

The form factor vanishes for wavelengths much shorter than the bunch length. The emitted transition radiation is then incoherent and its intensity scales with the number of particles N in a bunch. The incoherent part of the spectrum can be used to measure the transverse beam profile, the emittance and, by applying magnetic deflection, also the energy spread of the beam.
For wavelengths in the order of the bunch length or longer, the form factor approaches unity. Here the whole bunch appears as a single "macroparticle" of charge Ne. The emitted transition radiation is coherent and its intensity scales with N^2. The coherent part of the spectrum permits a direct measurement of $|f(\lambda)|^2$. It is obviously

much more intense than the incoherent part. To derive the longitudinal charge distribution by inverse Fourier transformation an assumption has to be made about the phase of $f(\lambda)$ as a function of λ. A possibility is to use a dispersion integral to relate the real and imaginary parts of $f(\lambda)$ [10]. Figure 1 shows several hypothetical longitudinal charge distributions and the corresponding coherent radiation spectra. The rms bunch length is 250 μm (left) respectively 50 μm (right) in each case.

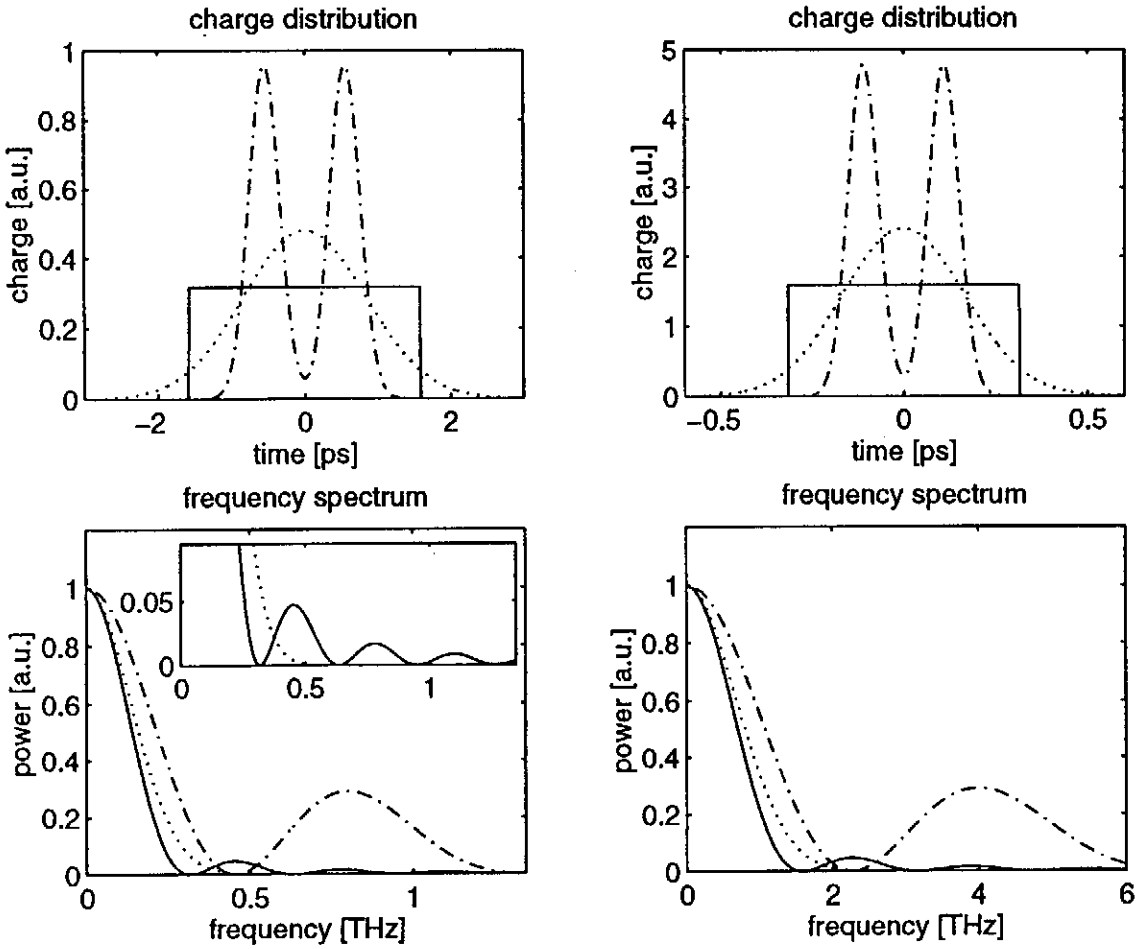

Figure 1: Hypothetical longitudinal charge distributions and the corresponding coherent radiation spectra. The plots on the left correspond to an rms bunch length of 250 μm, those on the right to 50 μm.

2.2 TTF Machine Parameters and Requirements on the Detector

The TTF photoinjector is designed to produce bunches of $6.3 \cdot 10^9$ electrons with a normalized emittance of 1 mm·mrad and an rms bunch length of σ_z = 1mm for Free Electron Laser (FEL) operation. The bunch repetition rate is 9 MHz, the overall length of the pulse train (macropulse) is 800 μs. Successive macropulses repeat every 100 ms (10 Hz). In the linac the bunch length is reduced by two compression stages, at energies of about 18 MeV and 140 MeV. The bunch length measurement will be performed behind the second compression stage where the expected rms bunch length is $\sigma_z = 250\mu$m (0.83 ps) [1]. The first FEL experiments will be performed at this bunch length. Later the TESLA Test Facility linac will be upgraded to a beam energy of 1 GeV for the operation of a vacuum ultraviolet FEL. Then a third compression stage is needed to reduce the bunch length to $\sigma_z = 50\mu$m (0.17 ps).

It has recently been demonstrated that a high-T_c Josephson junction cooled by liquid helium can operate in the frequency range from 50 to 2000 GHz [11]. With an improved optical coupling between radiation source and junction the range might be extended even to 5 THz. The frequency range of the detector is therefore fully adequate for measuring the bunch length for the charge distributions sketched above. The information on the shape of the distribution is contained in the high frequency tails of the spectrum, which are well within the dynamic range of the detector. A Josephson junction would hence permit reliable bunch length measurements at every compression stage along the TTF linac.

3 The Principle of Hilbert Transform Spectroscopy

A high-T_C Josephson junction serves as a Hilbert transform spectrometer. A Josephson junction consists of two superconducters separated by a thin insulating layer. The electrons in a superconductor form so-called Cooper-pairs which can be described by a single macroscopic quantum mechanical wave function. If the insulating layer is sufficiently thin, Cooper-pairs will penetrate from one superconductor to the other by the quantum mechanical tunnel effect. Equations describing the dynamics of the Josephson junction can be derived if one demands the continuity of the Cooper-pair wave function and its derivative across the junction. These so-called Josephson equations are

$$I_J = I_c \sin\phi(t) \tag{5}$$

$$\frac{d\phi}{dt} = \frac{2e}{\hbar}U(t) \tag{6}$$

where I_c is the critical current of the junction, $\phi(t)$ is the phase difference of the Cooper pair wave functions on both sides of the insulating layer and $U(t)$ is the voltage across the junction. The dc Josephson effect occurs for a time-independent phase. According to (6) U vanishes in this case and a dc Cooper-pair current I_J flows whose magnitude is $|I_J| \leq I_c$. The detection of microwave radiation is based on the ac Josephson effect, hence the junction is operated with a dc current $I = I_0 > I_c$, leading to a nonvanishing voltage U. Incident radiation modifies the current-voltage characteristic of the junction, and this change is used to determine the spectral distribution of the radiation.

Josephson junctions used for a spectral analysis of frequencies in the range 100-1000 GHz have to be designed to have a negligible capacitance. Their electrical performance is then well described by the so-called Resistively Shunted Junction (RSJ) model. An equivalent circuit is shown in Figure 2. Both Cooper pairs and unpaired

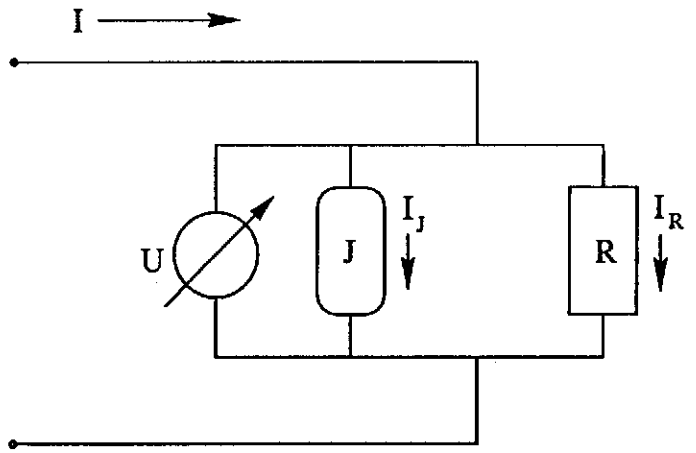

Figure 2: Equivalent circuit of a resistively shunted Josephson junction (RSJ model).

electrons are able to tunnel through the insulating layer of the Josephson junction. An applied current I splits up into a Cooper-pair (or Josephson) current (I_J) and a single-electron "resistive" current (I_R). The Cooper pair current obeys the Josephson equations.

3.1 DC Characteristic of the Josephson Junction

The equivalent circuit for an "autonomous" Josephson junction (without incident microwave radiation) is shown in Figure 2. The bias current of the junction is a pure dc current $I_0 > I_c$. According to Kirchhoff's law, the current I_0 splits into both branches of the circuit and the following equation holds:

$$I_0 = I_J + I_R = I_c \sin\phi + \frac{\hbar}{2eR}\frac{d\phi}{dt} . \tag{7}$$

Solving the differential equation for $\phi(t)$ and using equation (6), an expression for the time-dependent voltage $U(t)$ across the junction is derived. The result as shown in Appendix A is [12, 13]

$$U(t) = RI_c \cdot \frac{(I_0/I_c)^2 - 1}{I_0/I_c - \cos(\omega_0 t)} \quad \text{for} \quad I_0 > I_c \tag{8}$$

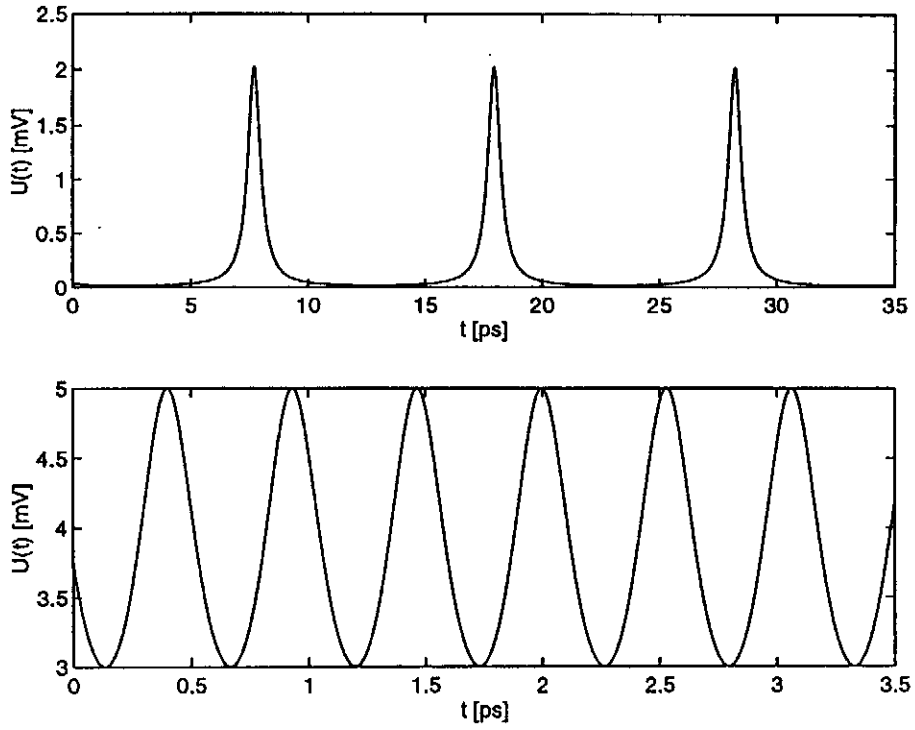

Figure 3: Time dependence of voltage U(t) across the Josephson junction for the autonomous case (no incident radiation). Top graph: $I_0/I_c = 1.02$, bottom graph: $I_0/I_c = 4$. The resistance R is assumed to be 1 Ω, the critical current is 1 mA.

where $\omega_0 = \frac{2e}{\hbar} R I_c \sqrt{(I_0/I_c)^2 - 1}$ is the Josephson frequency. An arbitrary constant phase has been omitted. This equation shows that for $I_0 > I_c$ an oscillating voltage $U(t)$ arises which derives from an alternating Cooper-pair current as well as a resistive single-electron current. The voltage $U(t)$ has a dc component but is not purely sinusoidal as can be seen from Figure 3. For a bias current just above the critical current a strongly distorted sine wave is observed while with increasing bias current the oscillation becomes more and more sinusoidal. Taking the time-average of Equation (8) one obtains (see Appendix A)

$$\overline{U} = \left\{ \begin{array}{ll} 0 & \text{for} \quad I_0 \leq I_c \\ R\sqrt{I_0^2 - I_c^2} & \text{for} \quad I_0 > I_c \end{array} \right\} . \tag{9}$$

The current-voltage characteristic of the junction, obtained by plotting I_0 as a function of $\overline{U}$, is shown as the dashed-dotted curve in Figure 4.

3.2 Josephson Junction with Incident Radiation

The incident microwave radiation is modelled by a small sinusoidal ac current which is superimposed with the dc bias current. We consider first the case of monochromatic radiation, the generalization to a continuous spectrum is straight forward. The total bias current is now the sum of a dc component I and an ac component with amplitude I_s and frequency $\omega_s/2\pi$

$$I(t) = I + I_s \sin \omega_s t \, . \tag{10}$$

The generalization of Equation (7) reads

$$I + I_s \sin \omega_s t = I_c \sin \phi + \frac{\hbar}{2eR} \frac{d\phi}{dt} \, . \tag{11}$$

The differential equation (11) has no analytic solution. It can be solved approximately if the amplitude I_s of the ac current, representing the incident radiation, is small compared to the dc bias current. A second-order perturbation approach [12, 13, 14], outlined in Appendix B, yields a correction to the dc current

$$\Delta I = -\frac{1}{4I} \left(\frac{2eRI_c}{\hbar} \right)^2 \cdot \frac{I_s^2}{\omega_s^2 - \omega_0^2} \quad \text{for} \quad (\omega_s \neq \omega_0) \tag{12}$$

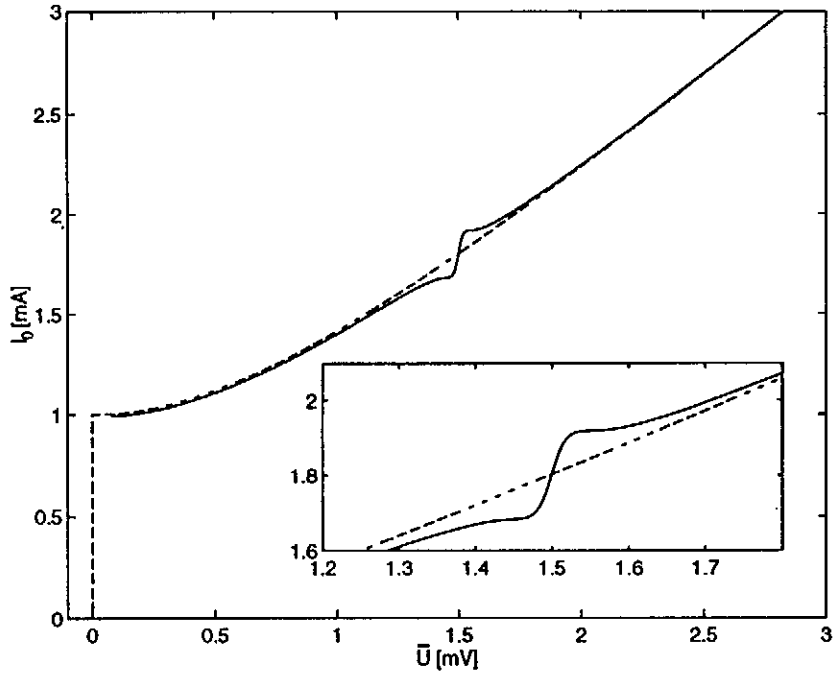

Figure 4: Dashed-dotted curve: time-averaged voltage across the junction as a function of the dc bias current. Solid curve: modification of dc characteristic curve due to monochromatic incident radiation. The dc current-voltage characteristic aquires a step at the voltage $\overline{U} = \hbar/2e\omega_s$. The height of the step is proportional to the incident radiation power. The RSJ model is assumed.

where

$$\omega_0 = \frac{2e\overline{U}}{\hbar} \tag{13}$$

denotes the frequency of the unperturbed Josephson oscillation at the given dc bias. The frequency ω_0 is often called the working point of the junction, since it gives the frequency of the unperturbed Josephson oscillation. The working point is changed by varying the dc bias current.

Equation (12) diverges for $\omega_0 = \omega_s$, but this divergence disappears if the internal noise in the junction is taken into account. With noise included the equation can be written as

$$\Delta I = -\frac{1}{8I\omega_0}\left(\frac{2eRI_c}{\hbar}\right)^2 \cdot \left(\frac{\omega_s - \omega_0}{(\omega_s - \omega_0)^2 + \gamma^2} - \frac{\omega_s + \omega_0}{(\omega_s + \omega_0)^2 + \gamma^2}\right) \tag{14}$$

where γ is a damping term introduced by the noise. Hence the junction responds to the incident monochromatic radiation in such a way that the dc current-voltage characteristic acquires a step ΔI in current at the voltage $\overline{U} = \hbar/2e\omega_s$. The height of the step is proportional to the incident radiation power. This is shown schematically in Figure 4.

3.3 Hilbert Transform Spectrometry

Incident radiation consisting of a number of discrete spectral lines will lead to corresponding discrete current steps in the I-U curve. Now we want to demonstrate that the Josephson junction, as described by the RSJ model, may equally well serve as a detector for electromagnetic radiation with a continuous spectral distribution $S_i(\omega_s)$ [6]. The basic point is the observation that the voltage response of the junction depends quadratically on the amplitude I_s of the ac current (see Equation (14)), hence intensities can be added. For this reason the voltage response to a continuous radiation spectrum is simply obtained by integrating Equation (12) over the frequency range of the radiation, taking the spectral intensity $S_i(\omega_s)$ as a weight factor.

$$\Delta I = -\left(\frac{2e}{\hbar}\right)^2 \frac{R^2 I_c^2}{4I} \int_0^\infty \frac{S(\omega_s)\, d\omega_s}{\omega_s^2 - \omega_0^2} \,. \tag{15}$$

The pole in the integrand requires a careful mathematical treatment (see Appendix B). The equation can be written in the following way

$$\Delta I = -\frac{1}{8I\omega_0}\left(\frac{2eRI_c}{\hbar}\right)^2 \mathcal{P}\int_{-\infty}^{\infty}\frac{S(\omega_s)\,d\omega_s}{\omega_s-\omega_0} = -\frac{\pi}{8I\omega_0}\left(\frac{2eRI_c}{\hbar}\right)^2 H[S(\omega_s)] \tag{16}$$

where $\mathcal{P}$ denotes the principal value of the integral and

$$H[S(\omega_s)] = \frac{1}{\pi}\,\mathcal{P}\int_{-\infty}^{\infty}\frac{S(\omega_s)\,d\omega_s}{\omega_s-\omega_0} \tag{17}$$

is the so-called Hilbert transform (see Appendix C) of the radiation spectrum $S(\omega_s)$. Note that by evaluating the principal value of the integral one can use the noise-free Equation (12) instead of (14). The spectral intensity of the incident radiation, computed by the inverse Hilbert transform of (16), is

$$S(\omega_s) = H^{-1}(g(\omega_0)) \tag{18}$$

with the function

$$g(\omega_0) = \frac{8}{\pi}\left(\frac{\hbar}{2e}\right)^2 \frac{\Delta I(\omega_0)I(\omega_0)\omega_0}{R^2 I_c^2}\,. \tag{19}$$

Equation (19) shows the quantities that have to be measured to determine the radiation spectrum. The current-voltage characteristic of the Josephson junction has to be scanned both with and without incident radiation. During the scan the bias current is increased in small steps. At each step the Josephson frequency $\omega_0 = 2eU/\hbar$ and the modification $\Delta U(\omega_0)$ due to the radiation are measured. The current modification ΔI is derived from ΔU via the differential resistance $R_d = d\overline{U}/dI$ of the unperturbed I-U curve. These quantities are used to compute the function $g(\omega_0)$ which is Hilbert-transformed to obtain the spectral intensity $S(\omega_s)$ of the incident radiation.

4 A first Measurement of Coherent Transition Radiation using Hilbert Transform Spectroscopy

A first experiment with a Josephson junction spectrometer at the TTF linac has been performed in August 1997. The linac was operated with a thermionic gun producing bunches with $2.3 \cdot 10^8$ electrons at a repetition rate of 216 MHz. The macropulse length was 30 μs and the macropulses repeated every 2 Hz. Using compression by a sub-harmonic buncher and a superconducting TESLA cavity an rms bunch length of $\sigma_z = 0.4$ mm (1.3 ps) was achieved [5, 15, 16].

The Experimental Setup

High-T_C Josephson junctions have been fabricated by epitaxial growth of $YBa_2Cu_3O_{7-x}$ on $NdGaO_3$ bicrystal substrates. A schematic view of the detector which incorporates the antennas for millimeter and submillimeter wave detection is shown in Figure 5. The size of the antenna varies from 1.8 mm at the outer bound to several micrometers at the center. Here, a grain boundary in the substrate cuts the thin film of the high-T_C superconductor, which then works as a Josephson junction. The electrical properties of grain boundary high-T_C junctions are very close to those predicted by the RSJ model [17, 18]. An electrical circuit to bias the junction with a dc current and to measure the potential difference across the contact is connected to the antennas. The junction features a large dynamic range of approximately 10^5 and a high sensitivity of $\approx 10^{-14}$ W/Hz$^{1/2}$ Noise Equivalent Power (NEP) to millimeter- and submillimeter radiation [19]. The resolution is around 1 GHz in the temperature range from 4 to 78 K [18].

The Josephson spectrometer was mounted at the same diagnostic station of the linac which had been used to determine the bunch length with a Martin-Puplett interferometer [5]. Transition radiation generated at the front face of an aluminum foil was guided through a quartz window to the antenna of the Josephson junction, using an arrangement of mirrors and wire grid polarizers. A grid served as a low pass filter for millimeter radiation. The Josephson junction was current-biased. The voltage response signal of the junction was amplified by a factor of 10^4, time-averaged by a digital oscilloscope and recorded as a function of the unperturbed Josephson frequency ω_0, derived from the time-averaged junction voltage $\overline{U}$. The operation of the spectrometer was controlled by a personal computer through an IEEE-488 interface.

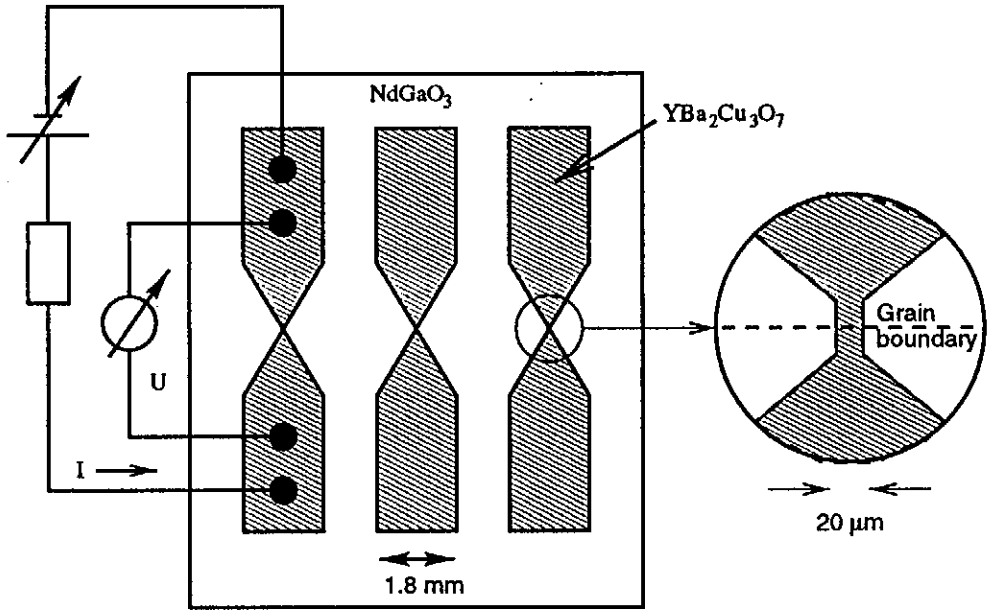

Figure 5: A schematic view of the Josephson junction used as a detector for millimeter and submillimeter wave radiation.

The Intrinsic Parameters of the Junction

Figure 6 shows the characteristic I-U curve of the Josephson junction used. The measured data points are presented as circles. For large bias currents an Ohmic characteristic is observed (linear relation between potential difference and bias current). The intrinsic parameters I_c and R of the junction are measured by fitting the theoretical I-U curve (9) to the data. The result is

$$I_c = 0.11 \text{ mA} \qquad R = 1.62\ \Omega\ . \tag{20}$$

The fit is shown as the dashed-dotted line in Figure 6a. The agreement with the data is quite satisfactory except in the vicinity of I_c where a gradual increase of the voltage is measured instead of the steep rise predicted by theory. The difference is due to noise in the junction. A better representation of the experimental I-U curve is obtained if the theoretical curve is convoluted with a Gaussian noise distribution.

$$\overline{U}(I) = \frac{1}{\sqrt{(2\pi\sigma^2)}} \int R\sqrt{I'^2 - I_c^2}\, \exp\left(-\frac{(I'-I)^2}{2\sigma^2}\right) dI'\ . \tag{21}$$

The variance σ is a fit parameter. The resulting solid curve in Figure 6a, corresponding to $\sigma = 0.02$ mA, provides a perfect description of the data.

The differential resistance of the junction $R_d = d\overline{U}/dI$ is computed by differentiation of the I-U curve with noise (21) or by taking the slopes between adjacent data points. Figure 6b shows that both methods are in good agreement. In the further analysis, the differential resistance obtained from the I-U fit curve is used to avoid the point-to-point fluctuations in the data.

The Spectroscopic Measurement

Figures 6 and 7 summarize the analysis of the spectroscopic measurements. The characteristic curve of the junction without incident radiation is shown in Figure 6. The spectroscopic information is contained in the difference $\Delta\overline{U}$ between the characteristic curves with and without radiation, which is shown in the upper graph in Figure 7. $\Delta\overline{U}$ is transformed to ΔI by $\Delta I = \Delta\overline{U}/R_d$, where R_d is the differential resistance shown in Figure 6b. The detector current response ΔI, the dc bias current I and the time-averaged voltage across the junction $\overline{U}$ are multiplied together to compute the characteristic function $g(\omega_0)$ as defined in Equation (19). $g(\omega_0)$ is shown in the lower plot in Figure 7. The determination of ΔI is problematic for small frequencies (i. e. dc bias currents close to I_c). The differential resistance R_d drops to zero when I approaches I_c so the data at small values of $\overline{U}$ are quite sensitive to small measurement errors and noise in the junction which has a significant influence on the differential resistance in the vicinity of I_c. Therefore the frequency range $0 < f_0 < 5$ GHz has been omitted from the present analysis.

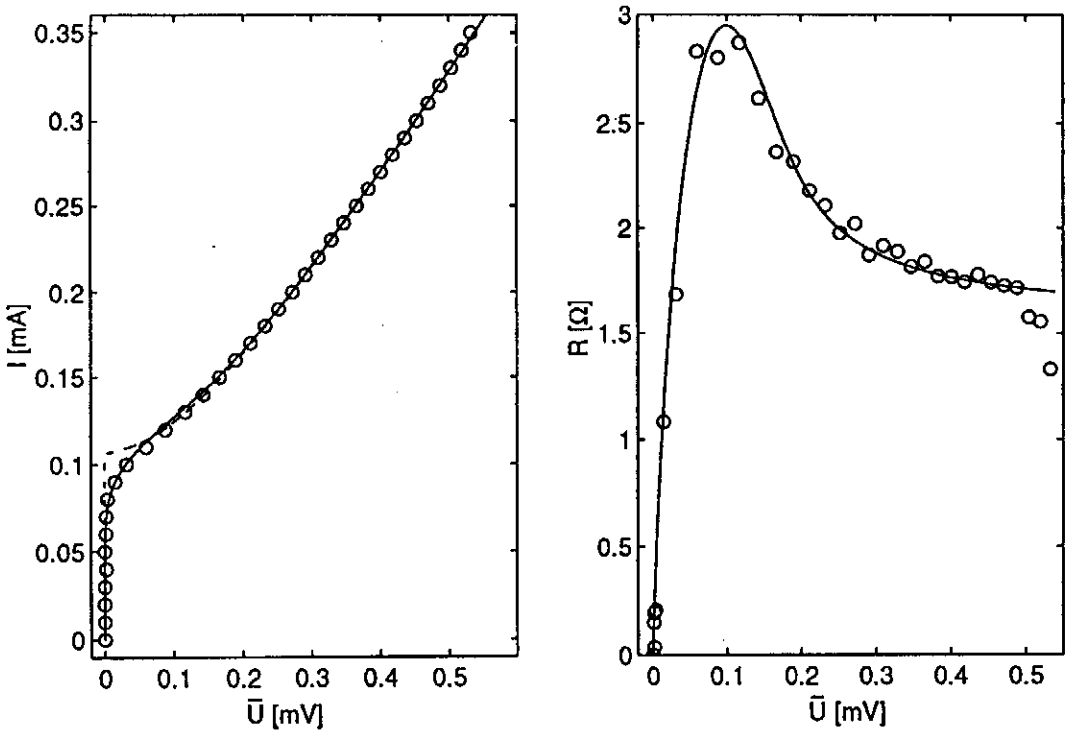

Figure 6: (a) The current-voltage characteristic of the Josephson junction without incident radiation. Measured data points are marked by circles. Dashed-dotted line: the theoretical I-U curve (9) with fitted values for I_c and R. Solid curve: convolution of theoretical I-U curve with Gaussian-distributed noise. (b) The differential resistance R_d as determined from differentiation of the I-U characteristic (solid curve), compared with point-to-point difference quotients (circles).

Since, however, $g(\omega_0)$ is needed at all frequencies to perform the Hilbert transform, a smooth extrapolation function of the form

$$g(\omega_0) \propto \frac{\omega_0}{\omega_0^2 + const} \quad \text{for} \quad f_0 = \omega_0/(2\pi) < 5 \text{ GHz} . \tag{22}$$

is used in the range $0 < f_0 < 5$ GHz, shown as a solid curve in Figure 7. The extrapolation function has to vanish at $\overline{U} = 0$ to generate an antisymmetric characteristic function $g(\omega_0)$. The Hilbert transformation of $g(\omega_0)$ then leads to a symmetric power spectrum.

The intensity spectrum was calculated using an algorithm of discrete Hilbert-transform [20]. Figure 8 shows the evaluated coherent radiation spectrum. The spectrum is plotted in the frequency range between 60 and 260 GHz. The power spectrum has a maximum at a frequency close to 100 GHz. The decrease towards smaller frequencies is explained by transmission losses of the radiation for frequencies close to cut-off frequency (60 GHz) of the WR-10 waveguide. The minimum at $f = (170 \pm 10)$ GHz is due to a water absorption line. The absorption loss can be corrected by adding a Lorentz resonance curve. The data shown in Figure 9 include this correction.

Data Analysis:

The main uncertainty of the present, preliminary, experiment originates from the wavelength-dependant acceptance of the transmission line-detector system. The point-to-point errors of the measurement are dominated by the read-out errors of the voltage response ΔU of the junction. These values were determined from a digital oscilloscope after averaging over 15 seconds. The precision of the read-out of the Josephson voltage is estimated to be better than 1 μV, the bias current power supply stability to 1 μA. The errors in the quantities U, I and ΔI are carried through the Hilbert transform and result in the error bars of the frequency spectrum shown Figure 9.
For the further analysis a Gaussian-shaped frequency spectrum of the radiation is assumed since figure 1 demonstrates that this is a good approximation if finer details of the bunch charge distribution are disregarded. The Gaussian fit applied to the data, shown as a solid line in figure 9, results in

$$\sigma_f = (98 \pm 16) \text{ GHz} . \tag{23}$$

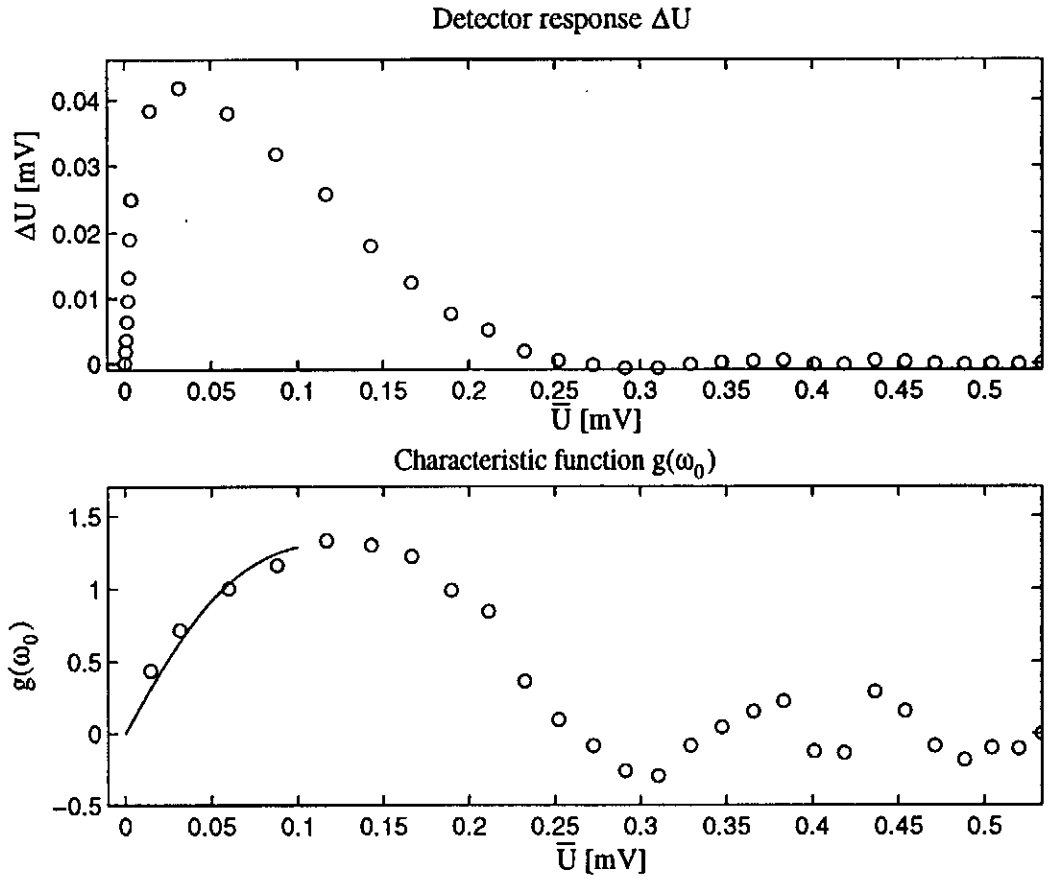

Figure 7: The analysis of the spectroscopic measurement to obtain the coherent transition radiation spectrum. The measured characteristic I-U curve of the Josephson junction without radiation is shown in Figure 6. Upper graph: The detector response ΔU as a function of $\overline{U}$. Lower graph: The characteristic function $g(\omega_0)$, as defined by Equation (19), plotted versus $\overline{U} = \hbar/2e\omega_0$. The solid line shows the extrapolation of $g(\omega_0)$ for small $\overline{U}$.

The variance refers to the intensity spectrum which is proportional to the square of the form factor. The rms bunch length is therefore given by

$$\sigma_t = \frac{1}{2\pi\sqrt{2}\sigma_f} = (1.2 \pm 0.2)\ \text{ps}\ . \tag{24}$$

Hence, the bunch length in the TTF linac as evaluated from this first preliminary measurement with the Josephson junction detector is

$$\sigma_z = c\sigma_t = (0.45 \pm .09)\ \text{mm}\ . \tag{25}$$

This is in reasonable agreement with other bunch length measurements.

5 Conclusion and Outlook

A Josephson junction can be used as a frequency-selective detector for millimeter and submillimeter wave radiation. The applicability for bunch length measurements at an electron linac has been demonstrated. It is planned to improve the Josephson-junction detector by mounting it in an optical cryostat with direct optical coupling to the radiation target. The read-out electronics will be adapted to a bandwidth sufficient to measure selected bunches within TTF macropulses. The Josephson spectrometer will be set up in parallel with a Martin-Puplett interferometer to have a direct comparison of both methods. The following measurements should be possible:

- A measurement of a particular bunch in the macropulse where the apparatus is triggered on the same bunch at every beam crossing. The I-U curve is sampled at one bias current per macropulse. In between the macropulses, measurements without radiation are taken. A measurement of 100 different frequencies would take about 10 seconds.

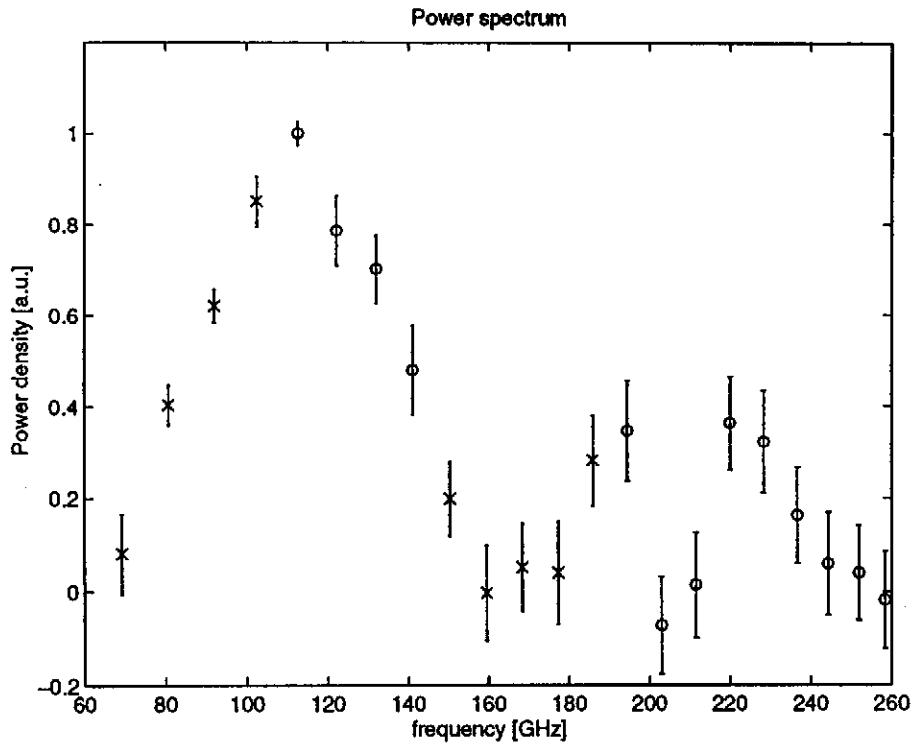

Figure 8: The coherent radiation spectrum as obtained from a discrete Hilbert transform of the characteristic function g. Corrections must be applied for data points marked with crosses. The decrease below $f = 100$ GHz is due to the WR-10 waveguide cut-off. These data points are not used in the analysis. The minimum at $f = (170 \pm 10)$ GHz originates from a water absorption line and can be corrected by adding a Lorentz resonance curve.

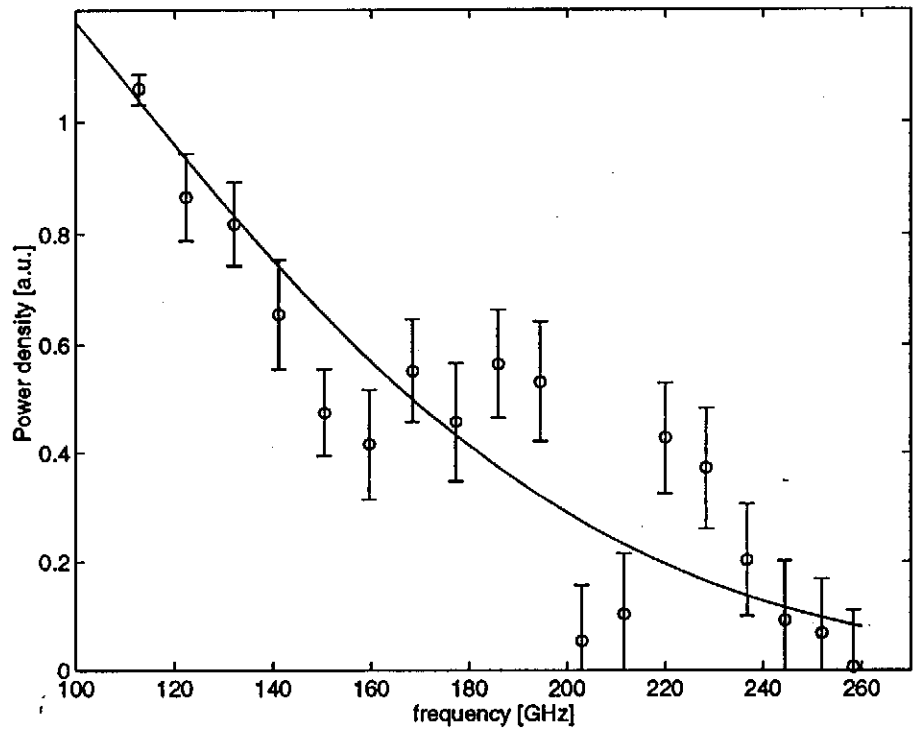

Figure 9: The coherent radiation spectrum for the TTF beam. A Gaussian fit is applied to the data yielding $\sigma_f = (98 \pm 16)$ GHz.

- The other option is a measurement of the average bunch length in a macropulse. Here, the I-U curve is sampled by changing the bias current in the 1 μs breaks between consecutive bunches. The measurement without radiation is taken either between bunch crossings or after the complete I-U curve has been scanned. This measurement will take 800 μs and yields 800 points in frequency space.

A Current-Voltage Characteristic without Radiation

A Josephson junction obeying the RSJ model is described by Equation (7)

$$I_0 = I_c \sin\phi + \frac{\hbar}{2eR}\frac{d\phi}{dt}.$$

A constant dc current $I_0 > I_c$ is applied. In the following we use dimensionless quantities

$$i_0 = I_0/I_c, \qquad u = U/RI_c, \qquad \tau = t\omega_c, \qquad \omega_c = \frac{2eRI_c}{\hbar}. \tag{26}$$

Equation (7) then transforms to

$$\frac{d\phi}{d\tau} = i_0 - \sin\phi(\tau)\,. \tag{27}$$

For $I_0 > I_c$, i.e. $i_0 > 1$, one gets $d\phi/d\tau = i_0 - \sin\phi(\tau) \neq 0$ so we can separate variables:

$$\frac{d\phi}{i_0 - \sin\phi} = d\tau\,. \tag{28}$$

Integration gives

$$\frac{2}{\sqrt{i_0^2-1}}\arctan\left(\frac{i_0\tan(\phi/2)-1}{\sqrt{i_0^2-1}}\right) = \tau + \text{const} \tag{29}$$

or

$$\tan(\phi/2) = \frac{1}{i_0} + \frac{\sqrt{i_0^2-1}}{i_0}\tan\left(\frac{\sqrt{i_0^2-1}}{2}\tau + \chi\right) \tag{30}$$

where χ is an arbitrary phase. Then ϕ is

$$\phi(\tau) = 2\arctan\left(\frac{1}{i_0} + \frac{\sqrt{i_0^2-1}}{i_0}\tan\left(\frac{\sqrt{i_0^2-1}}{2}\tau + \chi\right)\right)\,. \tag{31}$$

The normalized voltage is $u(\tau) = d\phi/d\tau$:

$$\begin{aligned} u(\tau) &= i_0 - (i_0^2-1)\frac{1+\tan^2\left(\frac{\sqrt{i_0^2-1}}{2}\tau+\chi\right)}{i_0 + \frac{1}{i_0}\left(1+\sqrt{(i_0^2-1)}\tan\left(\frac{\sqrt{i_0^2-1}}{2}\tau+\chi\right)\right)^2} \\ &= (i_0^2-1)\frac{1}{i_0 + \frac{1}{i_0}\left(\cos\left(\sqrt{i_0^2-1}\,\tau+2\chi\right)+\sqrt{(i_0^2-1)}\sin\left(\sqrt{i_0^2-1}\,\tau+2\chi\right)\right)}. \end{aligned} \tag{32}$$

The last expression can be simplified by substituting $\sin\theta = 1/i_0$ (remember that $I_0 > I_c$, so $i_0 > 1$). Then $\cos\theta = \sqrt{1-\sin^2\theta} = \frac{1}{i_0}\sqrt{i_0^2-1}$ and

$$u = \frac{(i_0^2-1)}{i_0 + \sin\left(\sqrt{i_0^2-1}\,\tau + 2\chi + \theta\right)}. \tag{33}$$

The constant χ is determined by the initial conditions. For the following calculations χ is chosen such that

$$u = \frac{(i_0^2-1)}{i_0 - \cos\left(\sqrt{i_0^2-1}\,\tau\right)}\,. \tag{34}$$

Returning to unnormalized quantities we get Equation (8). The dc voltage measured across the junction is the time-average of u(τ):

$$\overline{u} = \frac{1}{\tau_0}\int_0^{\tau_0}\frac{i_0^2-1}{i_0 - \cos\left(\sqrt{i_0^2-1}\,\tau\right)}d\tau\,. \tag{35}$$

Here $\tau_0 = 2\pi/\sqrt{i_0^2 - 1}$ is the period of oscillation. The integral yields

$$\overline{u} = \frac{2}{\tau_0}\left[\arctan\left(\frac{(i_0 - 1)\tan\left(\sqrt{i_0^2 - 1}\,\frac{\tau}{2}\right)}{\sqrt{i_0^2 - 1}}\right)\right]_{\tau=0}^{\tau=\tau_0} . \tag{36}$$

The argument of the tangent function is zero at the lower boundary and π at the upper boundary. The arctan function advances by π between two successive zeros of its argument. Therefore we obtain the simple formula

$$\overline{u} = \frac{2}{\tau_0}\pi = \sqrt{i_0^2 - 1} . \tag{37}$$

The result can be summarized by

$$\overline{u} = \left\{\begin{array}{ll} 0 & \text{for } |i_0| \le 1 \\ \sqrt{i_0^2 - 1} & \text{for } |i_0| > 1 \end{array}\right\} \tag{38}$$

and corresponds to Equation (9) in unnormalized quantities.

B Current-Voltage Characteristic with Radiation

Incident radiation is modelled by an additional sinusoidal current with amplitude I_s and frequency ω_s, which has to be superimposed on the dc bias current I. In normalized quantities, the differential Equation (11) becomes

$$i + i_s \sin(\Omega\tau) = \sin\phi(\tau) + \frac{d\phi}{d\tau} \tag{39}$$

with

$$i_s = \frac{I_s}{I_c} \quad \text{and} \quad \Omega = \frac{\omega_s}{\omega_c} . \tag{40}$$

Equation (39) has no analytical solution. The radiation-induced current can be regarded as a small perturbation since $i_s \ll 1$ [12]. In the following calculation we determine the change in the dc bias current while keeping the time-averaged voltage $\overline{u}$ constant (compare figure 4). The dc current i and the phase ϕ are expanded into powers of the ac-current amplitude i_s

$$i = i_0 + \sum_{k=1}^{\infty} a_k i_s^k \quad \text{and} \quad \phi = \phi_0 + \sum_{k=1}^{\infty} b_k i_s^k . \tag{41}$$

The $\sin\phi$ term in Equation (39) is expanded into a second-order Taylor series

$$\sin\left(\phi_0 + \sum_{k=1}^{\infty} b_k i_s^k\right) \approx \sin\phi_0 + b_1\cos\phi_0\, i_s + \left(b_2\cos\phi_0 - \frac{b_1^2}{2}\sin\phi_0\right) i_s^2 . \tag{42}$$

Equations (41) and (42) are introduced into the differential Equation (39). Sorting for powers of i_s we get

$$\frac{d\phi_0}{d\tau} + \sin\phi_0 = i_0 \tag{43}$$

$$\frac{db_1}{d\tau} + b_1\cos\phi_0 = a_1 + \sin(\Omega\tau) \qquad \text{for} \quad k = 1 \tag{44}$$

$$\frac{db_2}{d\tau} + b_2\cos\phi_0 = a_2 + \frac{b_1^2}{2}\sin\phi_0 \qquad \text{for} \quad k = 2 . \tag{45}$$

Equation (43) describes the characteristic of the junction without radiation and is solved by (31). Equations (44) and (45) are of the form

$$\frac{db_k}{d\tau} + b_k\cos\phi_0 = f_k(\tau) . \tag{46}$$

The general solution of this equation is

$$b_k = \exp\left(-\int^{\tau}\cos\phi_0\, d\tau'\right)\left(\int^{\tau}\exp\left(\int^{\tau'}\cos\phi_0\, d\tau''\right) f_k(\tau')\, d\tau'\right) . \tag{47}$$

An expression for $\cos\phi_0$ can be derived from (27). Taking the derivative with respect to the normalized time

$$\frac{d^2\phi_0}{d\tau^2} + \frac{d\phi_0}{d\tau}\cos\phi_0 = 0$$

one obtains

$$\cos\phi_0 = -\frac{\ddot{\phi}_0}{\dot{\phi}_0} = -\frac{d\ln\dot{\phi}_0}{d\tau}\,. \tag{48}$$

Inserting Equation (48) into (47) the latter equation yields

$$b_k = \dot{\phi}_0 \int^{\tau} \frac{f_k(\tau')}{\dot{\phi}_0(\tau')}\,d\tau'\,. \tag{49}$$

We are now looking for the change in the dc current at a fixed value of the time-averaged voltage:

$$\overline{u} = \overline{\dot{\phi}_0} + \overline{\dot{b}_1} + \overline{\dot{b}_2} + \ldots\ldots = \overline{\dot{\phi}_0}\,. \tag{50}$$

This is fulfilled if

$$\overline{\dot{b}_k} = 0 \quad \text{for all} \quad k > 0\,. \tag{51}$$

A consequence is that the integrand in Equation (49) is not allowed to have a dc component. This can be seen as follows. We form the long-term time average of $\dot{b}_k$

$$\overline{\dot{b}_k} = \lim_{T\to\infty}\frac{1}{T}\int_0^T \dot{b}_k d\tau = \lim_{T\to\infty}\frac{1}{T}(b_k(T) - b_k(0))\,. \tag{52}$$

Assume now that the integrand in Equation (49) had a dc component, say A. Then $b_k(T) - b_k(0)$ would be of the form $A\cdot T$ plus a bounded term due to the ac components of the integrand in (49). From the condition $\overline{\dot{b}_k} = 0$ follows immediately $A = 0$, i.e. the dc component is indeed zero.
The condition $\overline{\dot{b}_1} = 0$ implies

$$\overline{(a_1 + \sin(\Omega\tau))\,\dot{\phi}_0^{-1}} = 0 \tag{53}$$

or

$$\overline{(a_1 + \sin(\Omega\tau))\,(i_0 - \cos(\overline{u}\tau))} = 0 \tag{54}$$

where $f_1(\tau) = a_1 + \sin(\Omega\tau)$ has been inserted. Keeping in mind that a_1 describes a pure dc current component, Equation (54) can be solved for a_1:

$$a_1 = \frac{1}{i_0}\overline{\sin(\Omega\tau)\cos(\overline{u}\tau)} \quad \Rightarrow \quad a_1 = 0 \;\text{ for }\; \Omega \neq \overline{u}\,. \tag{55}$$

From Equation (55) follows directly that there is no first-order dc current component is introduced by the small ac current[1]. The first-order phase correction $b_1(\tau)$ can now be calculated from Equation (49) setting $a_1 = 0$. It follows

$$b_1 = \dot{\phi}_0 \int^{\tau} \frac{\sin(\Omega\tau')}{\dot{\phi}_0}d\tau' = \frac{1}{i_0 - \cos(\overline{u}\tau)}\int^{\tau}(i_0 - \cos(\overline{u}\tau'))\sin(\Omega\tau')\,d\tau' \tag{56}$$

or

$$b_1 = -\frac{1}{i_0 - \cos(\overline{u}\tau)}\left(\frac{i_0\cos(\Omega\tau)}{\Omega} - \frac{\cos((\Omega-\overline{u})\tau)}{2(\Omega-\overline{u})} - \frac{\cos((\Omega+\overline{u})\tau)}{2(\Omega+\overline{u})}\right)\,. \tag{57}$$

The next step is the solution of Equation (45) with the condition $\overline{\dot{b}_2} = 0$. The absence of a dc component in the integrand in (49) means for $k = 2$:

$$\overline{\left(a_2 + \frac{b_1^2}{2}\sin\phi_0\right)(i_0 - \cos(\overline{u}\tau))} = 0 \tag{58}$$

An expression for $\sin\phi_0$ can be derived from Equations (34) and (27).

$$\dot{\phi}_0 = \frac{\overline{u}^2}{i_0 - \cos(\overline{u}\tau)} = i_0 - \sin\phi_0 \tag{59}$$

and therefore

$$\sin\phi_0 = \frac{1 - i_0\cos(\overline{u}\tau)}{i_0 - \cos(\overline{u}\tau)}\,. \tag{60}$$

[1] A finite value is obtained for a_1 if $\Omega = \overline{u}$. This special case is excluded by taking the principal value of the integral in Equation (67)

Inserting the latter expression into Equation (58) and solving for the second-order correction a_2 of the dc current we find

$$a_2 = -\frac{1}{2i_0}\overline{(1 - i_0\cos(\overline{u}\tau))\, b_1^2}\,. \tag{61}$$

Now expression (57) has to be substituted for b_1 and with the identity

$$\frac{1 - i_0\cos\left(\sqrt{i_0^2-1}\,\tau\right)}{\left(i_0 - \cos\left(\sqrt{i_0^2-1}\,\tau\right)\right)^2} = -2\sum_{k=1}^{\infty}\frac{k\cos\left(k\sqrt{i_0^2-1}\,\tau\right)}{\left(i_0+\sqrt{i_0^2-1}\right)^k} \tag{62}$$

the following expression for the second-order dc current is found

$$a_2 = \frac{1}{a_0}\sum_{k=1}^{2}\frac{k\cos\left(k\sqrt{i_0^2-1}\,\tau\right)}{\left(i_0+\sqrt{i_0^2-1}\right)^k}\overline{\left(\frac{i_0\cos(\Omega\tau)}{\Omega} - \frac{\cos((\Omega-\overline{u})\,\tau)}{2(\Omega-\overline{u})} - \frac{\cos((\Omega+\overline{u})\,\tau)}{2(\Omega+\overline{u})}\right)^2}\,. \tag{63}$$

Note that only the first two terms ($k = 1, 2$) of the sum are included in taking the time average. Three terms have to be evaluated

$$\begin{aligned}
T_1 &= \frac{1}{\tau}\int^{\tau}\frac{1}{i_0(i_0+\overline{u})}\left(\frac{-a_0\cos^2(\Omega\tau')\cos^2(\overline{u}\tau')}{\Omega(\Omega-\overline{u})}\right)d\tau' \\
T_2 &= \frac{1}{\tau}\int^{\tau}\frac{1}{i_0(i_0+\overline{u})}\left(\frac{-a_0\cos^2(\Omega\tau')\cos^2(\overline{u}\tau')}{\Omega(\Omega+\overline{u})}\right)d\tau' \\
T_3 &= \frac{1}{\tau}\int^{\tau}\frac{2}{i_0(i_0+\overline{u})^2}\left(\frac{\left(\cos^2(\overline{u}\tau')\cos^2(\Omega\tau') - \sin^2(\overline{u}\tau')\sin^2(\Omega\tau')\right)\left(\cos^2(\overline{u}\tau') - \sin^2(\overline{u}\tau')\right)}{2(\Omega^2-\overline{u}^2)}\right)d\tau'\,.
\end{aligned}$$

The integrations are straight forward and lead to

$$a_2 = T_1 + T_2 + T_3 = -\frac{1}{4i_0(\Omega^2-\overline{u}^2)}\,. \tag{64}$$

The important result is that in second order a non-zero dc current component remains after the integration. This leads to a resonance-type correction of the dc current-voltage characteristic of the Josephson junction. In terms of currents, the final result can be stated as

$$\Delta i = a_2 i_s^2 = -\frac{i_s^2}{4i_0(\Omega^2-\overline{u}^2)} \quad \text{for} \quad \overline{u} \neq \Omega\,. \tag{65}$$

Returning to unnormalized quantities we get Equation (12). The current correction in second order Δi is proportional to the square of the perturbing radiation amplitude i_s^2 and is sensitive to its frequency ω_s. The first property implies that the Josephson junction acts as a "quadratic detector", i. e. the detector response is proportional to the incident radiation power.

The generalization of Equation (65) to a continous radiation spectrum is straight forward. The response of the Josephson junction to monochromatic perturbation has to be convoluted with the normalized continuous power spectrum $\overline{s}(\Omega)$. Equation (65) then becomes

$$\Delta i = -\frac{1}{4i_0}\int_{-\infty}^{\infty}\frac{i_s^2\,\overline{s}(\Omega)}{\Omega^2-\overline{u}^2}\,d\Omega = -\frac{1}{4i_0}\int_{-\infty}^{\infty}\frac{s(\Omega)}{\Omega^2-\overline{u}^2}\,d\Omega \tag{66}$$

where $s(\Omega) = \overline{s}(\Omega)\, i_s^2$. Returning to unnormalized quantities and setting $S(\Omega) = s(\Omega)/I_c$ we get Equation (15).

Equation (66) has to be solved for the power spectrum $s(\Omega)$. Consider

$$\begin{aligned}
\int_0^{\infty}\frac{s(\Omega)2\overline{u}}{\Omega^2-\overline{u}^2}\,d\Omega &= \int_0^{\infty}\frac{s(\Omega)(-\Omega+\overline{u})}{\Omega^2-\overline{u}^2}\,d\Omega + \int_0^{\infty}\frac{s(\Omega)(\Omega+\overline{u})}{\Omega^2-\overline{u}^2}\,d\Omega \\
&= \int_{-\infty}^{0}\frac{s(\Omega)(\Omega+\overline{u})}{\Omega^2-\overline{u}^2}\,d\Omega + \int_0^{\infty}\frac{s(\Omega)(\Omega+\overline{u})}{\Omega^2-\overline{u}^2}\,d\Omega \\
&= \int_{-\infty}^{\infty}\frac{s(\Omega)}{\Omega-\overline{u}}\,d\Omega
\end{aligned}$$

where $s(\Omega) = s(-\Omega)$ is assumed. The latter integral diverges for $\Omega = \overline{u}$. A correct mathematical treatment, however, demands for a principal value integral, denoted by $\mathcal{P}$, to exclude the pole. Hence

$$\Delta i = -\frac{1}{8 i_0 \overline{u}} \mathcal{P} \int_{-\infty}^{\infty} \frac{s(\Omega)}{\Omega - \overline{u}} \, d\Omega. \tag{67}$$

Equation (67) corresponds to Equation (16) in the text. The principal value integral (67) is related to the Hilbert transform, a well defined integral transform. The Hilbert transformation is derived from Fourier theory in Appendix C.

C The Hilbert Transform

In this section the Hilbert transformation will be derived from Fourier theory. The Fourier integral is written in the following way [21]:

$$f(x) = \int_0^{\infty} (a(y) \cos xy + b(y) \sin xy) \, dy \tag{68}$$

where

$$a(y) = \frac{1}{\pi} \int_{-\infty}^{\infty} f(u) \cos yu \, du \tag{69}$$

$$b(y) = \frac{1}{\pi} \int_{-\infty}^{\infty} f(u) \sin yu \, du \tag{70}$$

Inserting Equation (69) and (70) into (68) we obtain

$$f(x) = \frac{1}{\pi} \int_0^{\infty} dy \int_{-\infty}^{\infty} f(u) \cos (y(u - x)) \, du \tag{71}$$

or written in complex form

$$f(x) = \mathrm{Re} \, \frac{1}{\pi} \int_0^{\infty} dy \int_{-\infty}^{\infty} f(u) \exp (iy(u - x)) \, du = \mathrm{Re} \, \Phi. \tag{72}$$

Calculating the imaginary part of Φ instead we obtain

$$g(x) = \mathrm{Im} \, \Phi = \frac{1}{\pi} \int_0^{\infty} dy \int_{-\infty}^{\infty} f(u) \sin (y(u - x)) \, du \tag{73}$$

or

$$g(x) = \int_0^{\infty} (b(y) \cos xy - a(y) \sin xy) \, dy \, . \tag{74}$$

The integral (74) is called the allied integral of Fourier's integral [22]. The allied integral is obtained by replacing $a(y)$ by $b(y)$ and $b(y)$ by $-a(y)$ in (68). The twice repeated formation of the allied Fourier integral leads to the negative of the original.

According to Equation (74) the Fourier coefficient $a(y)$ and $b(y)$ can be written in a different way:

$$a(y) = -\frac{1}{\pi} \int_{-\infty}^{\infty} g(u) \sin yu \, du \tag{75}$$

$$b(y) = \frac{1}{\pi} \int_{-\infty}^{\infty} g(u) \cos yu \, du \, . \tag{76}$$

Formally we obtain from Equation (73)

$$g(x) = \frac{1}{\pi} \lim_{\lambda \to \infty} \int_0^{\lambda} dy \int_{-\infty}^{\infty} f(u) \sin (y(u - x)) \, du \, . \tag{77}$$

Integration of the outer integral leads to

$$g(x) = \frac{1}{\pi} \lim_{\lambda \to \infty} \int_{-\infty}^{\infty} f(u) \frac{1 - \cos (\lambda(u - x))}{u - x} \, du. \tag{78}$$

For $\lambda \to \infty$, however, the term $\cos(\lambda(u-x))$ averages to zero. Hence

$$g(x) = \frac{1}{\pi} \mathcal{P} \int_{-\infty}^{\infty} \frac{f(u)}{u-x}\, du \tag{79}$$

where $\mathcal{P}$ denotes the principal value at $u = x$.

The inversion of Equation (79) is derived by inserting (75) and (76) into (68) following

$$f(x) = -\frac{1}{\pi} \int_0^{\infty} dy \int_{-\infty}^{\infty} g(u) \sin(y(u-x))\, du. \tag{80}$$

Following the previous steps we obtain

$$f(x) = -\frac{1}{\pi} \lim_{\lambda \to \infty} \int_{-\infty}^{\infty} g(u) \frac{1-\cos(\lambda(u-x))}{u-x}\, du. \tag{81}$$

The $\cos(\lambda(u-x))$ term can be neglected for $\lambda \to \infty$ and the following expressions have been derived

$$g(x) = \frac{1}{\pi} \mathcal{P} \int_{-\infty}^{\infty} \frac{f(u)}{u-x}\, du, \qquad f(x) = -\frac{1}{\pi} \mathcal{P} \int_{-\infty}^{\infty} \frac{g(u)}{u-x}\, du \tag{82}$$

The reciprocity expressed by (82) was first discovered by Hilbert. The Hilbert transformation can also be derived from Cauchy's integral theorem.

References

[1] TESLA - Collaboration, *TESLA Test Facility Linac - Design Report*, DESY-TESLA 95-01 (1995).

[2] T. Nakazato et al. , Phys. Rev. Lett. **63**, 1245 (1989).

[3] T. Takahashi et al. , Phys. Rev. E **48**, 4674 (1993), and references therein.

[4] H. Wiedemann, AIP Conf. Proc. 367, 293 (1996), and references therein.

[5] K. Hanke, *Beam Diagnostics using Coherent Transition Radiation at the TESLA Test Facility Linac*, DESY-TESLA 97-14 (1997).

[6] Y. Y. Divin, O. Y. Polyanski, A. Y. Shul'man, Sov. Tech. Lett. **6**, 454 (1980); Y. Y. Divin, O. Y. Polyanski, and A. Y. Shul'man, IEEE Trans. Magn. **19**, 613, (1983).

[7] C. J. Hirschmugl, M. Sagurton, G. P. Williams, *Multiparticle Coherence Calculations for Synchrotron-Radiation Emission*, Physical Review A, **Vol. 44**, No. 2 (1991).

[8] J. S. Nodvick, D. S. Saxon, *Suppression of Coherent Radiation by Electrons in a Synchrotron*, Physical Review, **Vol. 96**, No. 1 (1954).

[9] E. B. Blum, U. Happek, A. J. Sievers, *Observation of Coherent Synchrotron Radiation at the Cornell Linac*, Nucl. Instr. Meth. A307 (1991).

[10] R. Lai, A. J. Sievers, *On using the Coherent Far IR Radiation produced by a Charged-Particle Bunch to determine its Shape: I Analysis*, Nucl. Instr. Meth. A397 (1997).

[11] Y. Y. Divin, O. Y. Volkov, H. Schulz, U. Poppe, Extended Abstracts, 6th Int. Superconductive Electronics Conf. , V. 3, 174-176, Berlin (1997).

[12] K. K. Likharev, *Dynamics of Josephson Junctions and Circuits*, New York, Gordon and Breach, (1996).

[13] H. Kanter, F. L. Vernon, J. Appl. Phys. **43**, 3174 (1972).

[14] J. H. Hinken, *The Josephson Junction as a Spectral Detector*, in "Superconducting Quantum Electronics", Ed. V. Kose, Springer, (1989).

[15] K. Hanke, *Measurement of Picosecond Electron Bunches in a Linear Accelerator*, dissertation, Universität Hamburg (1997), also DESY-TESLA 97-19 (1997).

[16] A. Variola, *Bunch length Measurement using a Streak Camera*, in preparation.

[17] A. V. Andreev, Y. Y. Divin, V. N. Gubankov, I. M. Kotelyanski, V. B. Kravchenko, S. G. Zybtsev, E. A. Stepantsov, Physica **C 226**, 17 (1994).

[18] Y. Y. Divin, H. Schulz, U. Poppe, N. Klein, K. Urban, P. Shadrin, I. M. Kotelyanski, E. A. Stepantsov, Physica **C 256**, 149 (1996).

[19] Y. Y. Divin et. al. , Appl. Phys. Lett. **68** (11), 11 March 1996.

[20] MATLAB (R), The MathWorks, Inc., Version 4.2c, (1994).

[21] I. N. Bronstein, K. A. Sememdjajew, *Taschenbuch der Mathematik*, Leipzig, Teubner, (1979).

[22] E. C. Titchmarsh, *Introduction to the Theory of Fourier Integrals*, Oxford, Clarendon Press.